Electrical Generation of Pure Spin Currents in a Two-Dimensional Electron Gas

S. M. Frolov, A. Venkatesan,* W. Yu, and J. A. Folk†
Department of Physics and Astronomy, University of British Columbia, Vancouver, British Columbia V6T 1Z4, Canada
W. Wegscheider
Institüt fur Angewandte und Experimentelle Physik, Universität Regensburg, Regensburg, Germany
(Received 2 October 2008; published 19 March 2009)

Pure spin currents are generated and detected in micron-wide channels of a GaAs two-dimensional electron gas, using quantum point contacts in an in-plane magnetic field as injectors and detectors. The enhanced sensitivity to spin transport offered by a nonlocal measurement geometry enables accurate spin current measurements in this widely studied physical system. The polarization of the contacts is used to extract the quantum point contact g factor and provides a test for spontaneous polarization at 0.7 structure. The spin relaxation length in the channel is 30–50 μm over the magnetic field range 3–10 T, much longer than has been reported in GaAs two-dimensional electron gases but shorter than that expected from Dyakonov-Perel relaxation.

DOI: 10.1103/PhysRevLett.102.116802 PACS numbers: 73.23.−b, 72.25.−b

Interest in the physics of spin in solid state devices is driven both by the technological promise of spin electronics, and by the insights that may be gained by using spin currents as a probe into interacting electron systems [1]. Optical spin current measurements have advanced our understanding of spin relaxation, accumulation, and separation via spin-orbit interaction in a variety of bulk semiconductors and quantum wells [2–7]. Spin currents can also be generated and detected electrically using spin-selective contacts, enabling straightforward integration into circuits where device geometry and spin parameters are controlled by gates [8–15].

Devices defined by electrostatic gates in GaAs/AlGaAs two-dimensional electron gases (2DEGs) display an extraordinary variety of spin-related phenomena, and show technological promise for quantum dot-based quantum information processing [16]. These structures are typically studied by measuring the charge currents passing through them, but interpreting spin properties from such measurements can be difficult [11,12,17]. Questions as basic as the possibility of spontaneous spin polarization in one-dimensional constrictions, known as quantum point contacts (QPCs), remain unresolved [18]. Much greater sensitivity to spin properties can be achieved by measuring pure spin currents resulting from spin-resolved charge transport, but such measurements have not yet been integrated with gate-defined mesoscopic devices [8].

In this Letter, we present electrical measurements of pure spin currents in micron-wide channels of a GaAs 2DEG using QPCs as injectors and detectors [19,20]. The ability to change the channel geometry *in situ* using gate voltages enabled a measurement of spin relaxation length even for small contact polarizations. The relaxation lengths observed in this work, $\lambda_s = 30$–50 μm, are significantly longer than the values typically reported in GaAs 2DEGs because spin-orbit mediated relaxation was suppressed by the external magnetic field [21–23]. The temperature and field dependences of the pure spin current polarization were used to extract a Lande g factor in the QPCs, $|g| = 0.75 \pm 0.1$, that is enhanced compared to $|g| = 0.44$ in the bulk. This result contrasts with previous g factor measurements based on spin-polarized charge currents in QPCs [10,15]. No direct evidence of spin polarization was observed at zero magnetic field [18,24].

Pure spin currents are generated electrically through a sequence of two processes. First, charge is injected across a spin-selective barrier, creating a higher population of one spin. Next, the spin population that accumulates outside of the injector diffuses towards a large electrically floating reservoir with spins in equilibrium. Realizations of this technique often rely on ferromagnetic contacts [8,9,13,25], but injection from ferromagnets into GaAs 2DEGs remains a challenge. QPCs in Tesla-scale magnetic fields are a natural alternative because they are defined within the 2DEG itself, and have previously been shown to transmit spin-polarized currents by acting as a barrier for the higher-energy spin [10,19,20]. In contrast to ferromagnets, the QPC polarization axis is aligned with the external magnetic field so no Hanle precession of spin currents is expected.

In this experiment, a voltage applied across a spin-selective injector QPC drove polarized current I_{inj} into the center of a long channel [Fig. 1(a)]. The spin population that accumulated above the injector diffused toward the 2DEG reservoirs at the left and right ends of the channel. All charge current flowed to the electrical ground at the left; pure spin current flowed to the right. The detector QPC, located a distance x_{id} to the right of the injector, measured the nonlocal voltage, V_{nl}, due to spin accumulation generated by the pure spin current.

The devices were defined using electrostatic gates on the surface of a [001] GaAs/AlGaAs heterostructure. The

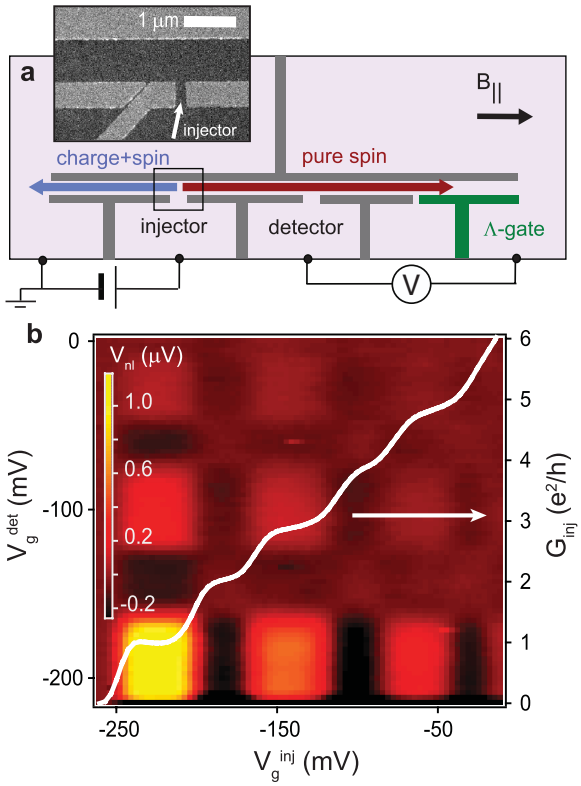

FIG. 1 (color). (a) Schematic of nonlocal measurement geometry. Depleted gate pattern (dark gray) simplified for clarity. Inset: scanning electron micrograph (SEM) of typical QPC (gates are light gray in SEM image). Nonlocal voltages reported in this paper are for the detector region with respect to the right reservoir. (b) Nonlocal voltage as injector (bottom axis) and detector (left axis) QPC's are scanned through polarized and unpolarized settings using V_g ($B_\parallel = 10$ T, $T = 500$ mK, $V_{ac} = 50\ \mu$V, $x_{id} = 6.7\ \mu$m). Injector conductance shown in white (right axis). Relative magnitudes of the signal at different spin-polarized squares reflect reduced polarization at higher odd QPC plateaus ($G = 3e^2/h, 5e^2/h, \ldots$), partially counteracted by higher injector currents in a voltage-biased configuration.

2DEG was 110 nm below the surface, with electron density $n_s = 1.11 \times 10^{11}$ cm^{-2} and mobility $\mu = 4.44 \times 10^6$ cm^2/V s measured at $T = 1.5$ K. The data in this Letter are from three channels, each along the [110] crystal axis, with lithographic width 1 μm and length 100 μm. The injector and detector spacing ranged from $x_{id} =$ 3–20 μm. Lock-in measurements in a dilution refrigerator were performed in magnetic fields $B_\parallel$ applied along the channel axis. To avoid trajectories dominated by skipping orbits, the out-of-plane component $B_\perp$ was kept under 50 mT, ensuring that the cyclotron radius was greater than the channel width. The effective sheet resistance in the channel, $\rho_\square \sim 20$–$120\ \Omega$, depended on cooldown conditions. The resistance increased by 10%–20% from $B_\parallel = 0$ to $B_\parallel = 10$ T.

Gate voltages control QPC conductance $G(V_g)$ and polarization $P(V_g)$. $G(V_g)$ is quantized in units of $1e^2/h$ at high magnetic field, as spin-resolved one-dimensional subbands are added one by one. The first ($G = 1e^2/h$) plateau corresponds to fully polarized transmission, $P = (G_\uparrow - G_\downarrow)/(G_\uparrow + G_\downarrow) \sim 1$, as only a single spin-up subband is allowed through the QPC ($G_\downarrow \sim 0$). The second ($G = 2e^2/h$) plateau corresponds to unpolarized transmission, $P = 0$ (one spin-up and one spin-down subband); the third corresponds to $P = 1/3$ (two spin-up and one spin-down subband), etc.

Nonlocal signals measured at high magnetic field had a characteristic signature of spin currents, see Fig. 1(b). Positive voltages indicating a nonequilibrium spin population above the detector were observed when both contacts were spin selective, i.e., when both were tuned to odd conductance plateaus (G_{inj}, $G_{det} = 1e^2/h$, $3e^2/h$, etc.). The voltage was near zero when both the detector and the injector were set to even plateaus (G_{inj}, $G_{det} = 2e^2/h$, $4e^2/h$, etc.). A small negative voltage was often observed when only the injector or only the detector was polarized (e.g., [$G_{inj} = 2e^2/h$, $G_{det} = 1e^2/h$] or [$G_{inj} = 1e^2/h$, $G_{det} = 2e^2/h$]). The origins of the negative signal are not understood.

The spin signal depends on diffusion, spin relaxation, and contact polarization. The expected magnitude of the nonlocal voltage can be calculated from a 1D diffusion equation $\partial^2 V_{nl}/\partial x^2 = V_{nl}/\lambda_s^2$ that assumes exponential spin relaxation, where the spin relaxation length λ_s depends on the diffusion constant and spin relaxation time [26]. The expression for V_{nl} is derived using the boundary conditions of equilibrium polarization at the left and right ends of the channel located at distances L_l and L_r from the injector [$V_{nl}(L_l) = V_{nl}(L_r) = 0$]:

$$V_{nl}(x_{id}) = \frac{\rho_\square \frac{\lambda_s}{w} I_{inj} P_{inj} P_{det} \sinh(\frac{L_r - x_{id}}{\lambda_s})}{\sinh(L_r/\lambda_s)(\coth(L_r/\lambda_s) + \coth(L_l/\lambda_s))} \quad (1)$$

where w is the channel width.

One way to measure spin relaxation length is to compare V_{nl} across several detectors at different positions along the channel, but this technique relies on identical detector polarizations—not necessarily the case for QPCs at low field and finite temperature. The flexibility of the gate-defined geometry enabled a measurement of λ_s that was independent of P_{inj} and P_{det}.

The bottom wall of the channel to the right of the detector was defined by two gates, see Fig. 1(a). Undepleting the Λ gate shortens the right side of the channel, bringing the right-hand equilibrium spin reservoir closer to the detector [Figs. 2(a) and 2(b)] and causing a faster drop in the spin-up chemical potential along the channel [Fig. 2(c)]. If the spin current has relaxed before reaching the Λ gate, the effect of undepleting the Λ gate is negligible. But for a channel with $\lambda_s \gtrsim L_r$, the nonlocal signal decreases when the Λ gate is undepleted [Fig. 2(d)], and λ_s can be extracted from the ratio of the signals for long and short channels using Eq. (1).

Two devices gave $\lambda_s = 30 \pm 10\ \mu$m and $\lambda_s = 50 \pm 10\ \mu$m, corresponding to channel resistivities of 20

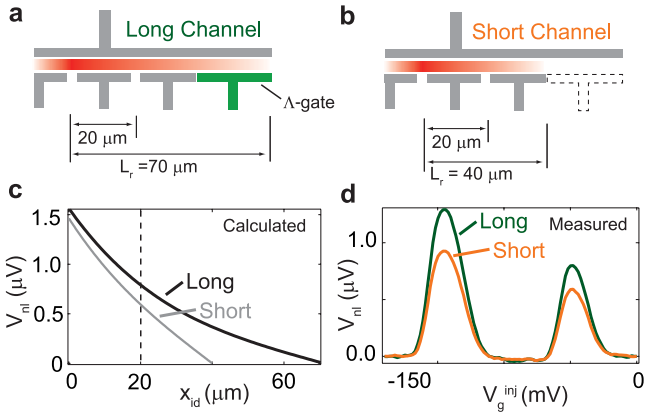

FIG. 2 (color online). (a) and (b) nonequilibrium spin-up chemical potential (gradient) in the 2DEG channel with Λ gate depleted (long) and undepleted (short). (c) Nonlocal voltage calculated from Eq. (1) for a range of injector-detector spacings, using $\lambda_s = 30\ \mu$m and the channel lengths in panels (a) and (b). (d) Nonlocal signal measured with Λ gate depleted and undepleted, for a device with $x_{\mathrm{id}} = 20\ \mu$m and the geometry of panels (a) and (b), using a polarized detector at $T = 1.2$ K.

and 50 Ω/sq, respectively [λ_s is reported here only for channels with uniform resistivity, a necessary condition for the validity of Eq. (1)]. The channel geometries were slightly different, preventing a correlation between resistivity and λ_{so} to be determined from this data. The spin relaxation length was independent of field and temperature from $B_{\|} = 3$–10 T and $T = 50$ mK–2 K.

The primary source of spin relaxation in GaAs 2DEGs is believed to be trajectory-dependent effective magnetic fields, B_{so}, arising from spin-orbit interaction, known as the Dyakonov-Perel (DP) mechanism [27]. Spins oriented by $B_{\|}$ along the [110] crystal axis relax due to the component of B_{so} along the $[\bar{1}10]$ axis, but relaxation is suppressed when $B_{\|} \gg B_{\mathrm{so}}$ [22,23]. Monte Carlo simulations of DP spin dynamics using the channel geometry from this work suggest an upper limit $B_{\mathrm{so}}[\bar{1}10] < 1.5$ T in order to find $\lambda_s > 30\ \mu$m over the field range $B_{\|} = 3$–10 T [28].

While experiment indicates the spin relaxation length of tens of microns, the simulations suggest that λ_s should rise to $>300\ \mu$m at $B_{\|} = 10$ T. This discrepancy may imply that mechanisms other than DP are at play. For example, momentum relaxation in spin-orbit coupled systems can lead to a field-independent spin relaxation length (the Elliott-Yafet mechanism) [29,30].

The ability to measure spin relaxation lengths independently means that the detected spin current can be used to quantify spin-selective transmission of the injector and detector. A simple model of a QPC is a saddle point potential barrier that couples two leads with thermally broadened Fermi distributions and Zeeman-split spin populations; the temperature dependence of spin transmission provides a direct measure of the g factor. In general, QPC polarization approaches $P = 1$ when Zeeman energy $g\mu_B B$ is much larger than both thermal broadening $k_B T$ and tunnel broadening $\hbar\omega$. Polarization results from different spin-resolved conductances:

$$G_{\uparrow[\downarrow]}(E_0) = \int \frac{df(E + [-]\frac{g\mu_B B_{\|}}{2}, T)}{dE} T(E - E_0) dE,$$

with subband cutoff energy $E_0(V_g)$ and transmission $T(E) = 1/(1 + e^{-2\pi E/\hbar\omega})$.

Over the past decade, conflicting reports of the g factor in QPCs have appeared in the literature. Some, primarily based on conductance signatures and shot noise measurements, have ascribed an enhanced g factor in low-density QPCs to exchange interaction [18,31]. In contrast, measurements of the spin-polarized charge currents have reported $|g| = 0.44$ as in the bulk [10,15]. The magnetic field and temperature dependence of the pure spin currents in this work gave $|g| = 0.75 \pm 0.1$ (Fig. 3), confirming the conclusions of conductance-based experiments.

Nonlocal voltages unrelated to spin accumulation were also observed. Fluctuations due to quantum interference were superimposed on the spin signal, but were within experimental noise for $x_{\mathrm{id}} > 10\ \mu$m or $T > 200$ mK [32]. Joule and Peltier heating of the channel by the injected current gave rise to a temperature difference across the detector, ΔT, that led to thermoelectric contributions to the nonlocal voltage [33,34]. Signals due to Joule heating did not interfere with the spin signal because they appeared at the second harmonic ($2f$) of the lock-in excitation, $\Delta V_{\mathrm{Joule}} = S_{\mathrm{det}} \Delta T \propto S_{\mathrm{det}} I_{\mathrm{inj}}^2$, where S_{det} is the thermopower of the detector QPC.

In contrast to Joule heating, Peltier heating appears at the first harmonic ($1f$) of the excitation: $\Delta V_{\mathrm{Peltier}} \propto S_{\mathrm{det}} S_{\mathrm{inj}} T I_{\mathrm{inj}}$, and was more difficult to distinguish from the spin signal. An identifying characteristic of the spin signal was its magnetic field dependence: the spin component was significantly larger than the thermoelectric voltage for $B_{\|} > 3$ T, but the distinction was ambiguous at lower fields. A nonlocal signal that remained clearly vis-

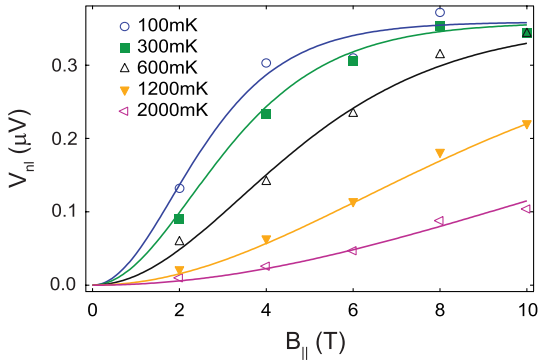

FIG. 3 (color online). Peak nonlocal signal for G_{inj} and G_{det} near $1e^2/h$, across a range of magnetic fields and temperatures. All data are from a single cooldown, with $V_{\mathrm{ac}} = 10\ \mu$V and $\rho_{\square} \sim 120\ \Omega$. Solid lines show fit of QPC model to data. Fits do not include data at zero field because the distinction between thermoelectric and spin signals was ambiguous (see text).

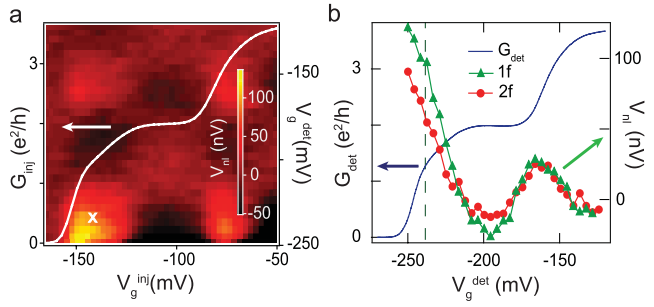

FIG. 4 (color). (a) Colorscale: first harmonic of the nonlocal signal at $B_{\|} = 0$. White trace shows conductance of injector QPC (left axis). Gate settings used to estimate Peltier coefficient indicated with "x". (b) $1f$ and $2f$ nonlocal signals (right axis) correlate with conductance of detector QPC (left axis), measured with injector QPC at "x" from (a). Dashed line indicates detector gate setting used to calibrate thermoelectric sensitivity. ($V_{ac} = 50\ \mu$V, $T = 500$ mK, $B_{\|} = 0$).

ible down to zero field in the experiment motivated a more careful analysis of the thermoelectric contribution.

Figure 4(a) illustrates the similarity between spin and thermal signatures at low magnetic field [cf. Fig. 1(b)]. QPC thermopower is zero on conductance plateaus, but finite at the transitions between plateaus as well as on the so-called 0.7 structure that is commonly observed at low field [18,33,35]. Finite thermopower for injector and detector near the steps in conductance gives rise to a Peltier signal in a checkerboard pattern that is reminiscent of the spin signal. The thermoelectric origin of the $1f$ signal in Fig. 4(a) is supported by a comparison of the zero-field signals at $1f$ and $2f$ [Fig. 4(b)]. The $2f$ signal is proportional to Joule heating by the injected current and to the thermopower of the detector, and serves as a fingerprint of thermal effects. The $1f$ signal shows a nearly identical gate voltage dependence to the $2f$ signal, suggesting that it is also thermal. The $2f$ signal can be used to extract the thermoelectric sensitivity of the detector QPC to heating: $V_{nl}/(I^2R) = 1 \pm 0.1$ nV/fW at the first detector conductance step. Assuming that the $1f$ signal is due entirely to Peltier heating through the injector, the magnitude of the signal at the first injector and detector conductance steps implies $S_{inj} = 100 \pm 10\ \mu$V/K at $T = 500$ mK, consistent with previous measurements [33,34,36].

Spin selectivity of QPCs at zero magnetic field has been linked to 0.7 structure in earlier experiments [18,24]. The analysis above shows that the data in Fig. 4(a) may be explained without invoking static spin polarization. In fact, no evidence for spin polarization was visible in the magnetic field dependence near zero field. For example, Hanle precession due to milli-Tesla–scale external fields would have been expected if the polarization axes of the QPCs were fixed by an intrinsic broken symmetry. If the polarization axes were not fixed, an increase in the signal might have been expected as uncorrelated axes were aligned by a small external magnetic field. To look for these effects, small fields were applied along [110] and [$\bar{1}$10], but no change in the signal was observed up to several hundred milli-Tesla, where conventional QPC polarization sets in.

The authors thank M. Duckheim, J. C. Egues, D. Loss, S. Lüscher, and G. Usaj for valuable discussions. Work at UBC supported by NSERC, CFI, and CIFAR. W. W. acknowledges financial support by the Deutsche Forschungsgemeinschaft (DFG) in the framework of the program "Halbleiter-Spintronik" (SPP 1285).

*Present address: School of Physics & Astronomy, University of Nottingham, Nottingham, NG72RD, U.K.
†To whom correspondence should be addressed. jfolk@physics.ubc.ca

[1] I. Zutic, J. Fabian, and S. Das Sarma, Rev. Mod. Phys. **76**, 323 (2004).
[2] Y. K. Kato *et al.*, Science **306**, 1910 (2004).
[3] S. A. Crooker *et al.*, Science **309**, 2191 (2005).
[4] V. Sih *et al.*, Phys. Rev. Lett. **97**, 096605 (2006).
[5] A. W. Holleitner *et al.*, Phys. Rev. Lett. **97**, 036805 (2006).
[6] C. P. Weber *et al.*, Phys. Rev. Lett. **98**, 076604 (2007).
[7] L. Meier *et al.*, Nature Phys. **3**, 650 (2007).
[8] M. Johnson and R. H. Silsbee, Phys. Rev. Lett. **55**, 1790 (1985).
[9] F. J. Jedema, A. T. Filip, and B. J. van Wees, Nature (London) **410**, 345 (2001).
[10] R. M. Potok *et al.*, Phys. Rev. Lett. **89**, 266602 (2002).
[11] J. A. Folk *et al.*, Science **299**, 679 (2003).
[12] L. P. Rokhinson *et al.*, Phys. Rev. Lett. **93**, 146601 (2004).
[13] S. O. Valenzuela and M. Tinkham, Nature (London) **442**, 176 (2006).
[14] N. Tombros *et al.*, Nature (London) **448**, 571 (2007).
[15] E. Koop *et al.*, Phys. Rev. Lett. **101**, 056602 (2008).
[16] K. C. Nowack *et al.*, Science **318**, 1430 (2007).
[17] R. Hanson *et al.*, Phys. Rev. B **70**, 241304(R) (2004).
[18] K. J. Thomas *et al.*, Phys. Rev. Lett. **77**, 135 (1996).
[19] B. J. van Wees *et al.*, Phys. Rev. Lett. **60**, 848 (1988).
[20] D. A. Wharam *et al.*, J. Phys. C **21**, L209 (1988).
[21] J. B. Miller *et al.*, Phys. Rev. Lett. **90**, 076807 (2003).
[22] E. L. Ivchenko, Fiz. Tverd. Tela **15**, 1566 (1973).
[23] M. Duckheim and D. Loss, Phys. Rev. B **75**, 201305 (2007).
[24] L. P. Rokhinson, L. N. Pfeiffer, and K. W. West, Phys. Rev. Lett. **96**, 156602 (2006).
[25] X. H. Lou *et al.*, Nature Phys. **3**, 197 (2007).
[26] F. J. Jedema *et al.*, J. Supercond. **15**, 27 (2002).
[27] M. I. Dyakonov and V. I. Perel, Sov. Phys. Solid State **13**, 3023 (1972).
[28] S. Lüscher, S. M. Frolov, and J. A. Folk (unpublished).
[29] R. Elliott, Phys. Rev. **96**, 226 (1954).
[30] F. X. Bronold *et al.*, Phys. Rev. B **66**, 233206 (2002).
[31] L. DiCarlo *et al.*, Phys. Rev. Lett. **97**, 036810 (2006).
[32] W. J. Skocpol *et al.*, Phys. Rev. Lett. **58**, 2347 (1987).
[33] L. W. Molenkamp *et al.*, Phys. Rev. Lett. **65**, 1052 (1990).
[34] L. W. Molenkamp *et al.*, Phys. Rev. Lett. **68**, 3765 (1992).
[35] N. J. Appleyard *et al.*, Phys. Rev. B **62**, R16 275 (2000).
[36] N. J. Appleyard *et al.*, Phys. Rev. Lett. **81**, 3491 (1998).